

Magnetic excitations and phonons in the spin-chain compound NaCu_2O_2

K.-Y. Choi,¹ V. P. Gnezdilov,² P. Lemmens,^{3,4} L. Capogna,^{5,6}

M. R. Johnson,⁶ M. Sofin,³ A. Maljuk,³ M. Jansen,³ and B. Keimer³

¹ *Institute for Materials Research, Tohoku University, Katahira 2-1-1, Sendai 980-8577, Japan*

² *B. I. Verkin Institute for Low Temperature Physics NASU, 61164 Kharkov, Ukraine*

³ *Max Planck Institute for Solid State Research, D-70569 Stuttgart, Germany*

⁴ *Institute for Physics of Condensed Matter, TU Braunschweig, D-38106 Braunschweig, Germany*

⁵ *CNR-INFM, CRS-SOFT and OGG Grenoble, 6 Rue J. Horowitz,*

BP 156 F-38042 Grenoble CEDEX 9, France and

⁶ *Institut Laue Langevin, 6 rue J. Horowitz BP 156 38042 Cedex 9 Grenoble, France*

(Dated: July 14, 2021)

We report an inelastic light scattering study of single-crystalline NaCu_2O_2 , a spin-chain compound known to exhibit a phase with helical magnetic order at low temperatures. Phonon excitations were studied as a function of temperature and light polarization, and the phonon frequencies are compared to the results of *ab-initio* lattice dynamical calculations, which are also reported here. The good agreement between the observed and calculated modes allows an assignment of the phonon eigenvectors. Two distinct high-energy two-magnon features as well as a sharp low-energy one-magnon peak were also observed. These features are discussed in terms of the magnon modes expected in a helically ordered state. Their polarization dependence provides evidence of substantial exchange interactions between two closely spaced spin chains within a unit cell. At high temperatures, the spectral features attributable to magnetic excitations are replaced by a broad, quasielastic mode due to overdamped spin excitations.

PACS numbers: 75.40.Gb, 63.20.-e, 78.30.-j, 75.50.-y

I. INTRODUCTION

A large research effort over the past three decades has been devoted to the exploration of quantum effects in spin-chain materials. At low temperatures, most quasi-1D magnets exhibit either gapped spin-liquid ground states, or states with collinear long-range magnetic order.¹ In some spin-chain compounds, spin-lattice interactions stabilize spin-Peierls ground states. Recently, several quasi-1D magnets with noncollinear, incommensurate long-range order at low temperatures have also been found. LiCu_2O_2 , an insulating compound containing edge-sharing CuO_2 chains, is a prominent example.^{2,3,4,5,6,7} Initially, both lattice disorder³ and spin frustration⁴ had been discussed as the driving mechanism of the observed helimagnetic order. This controversy now appears to have been resolved:⁶ The incommensurate magnetic ordering is due to long-range competing exchange interactions along the CuO_2 chains. Questions remain, however, about the microscopic role of the substantial number of Li impurities substituting copper ions on the spin chains, and about the magnitude of the exchange interactions between two closely spaced CuO_2 chains within a unit cell. Inelastic neutron scattering measurements⁵ suggest that these interactions are substantial, whereas electronic structure calculations⁴ indicate much smaller values.

Investigations of the disorder-free, isostructural compound NaCu_2O_2 ⁸ have now begun to help resolve these and other questions.⁹ This material is also interesting because it is the end member of the series $\text{Na}_{1+x}\text{Cu}_2\text{O}_2$. For nonzero x , the spin chains of these materials are doped

and exhibit intriguing phenomena such as Wigner crystallization of holes.¹⁰ Like its Li-analog, NaCu_2O_2 has an orthorhombic crystal structure with space group Pnma. The lattice parameters are $a=6.2087 \text{ \AA}$, $b=2.9343 \text{ \AA}$, and $c=13.0548 \text{ \AA}$.⁸ Magnetic Cu^{2+} ions form two inequivalent edge-sharing copper oxide chains per unit cell. They run along the b axis and are shifted relative to each other by $b/2$. Along the a and c -directions, they are separated by nonmagnetic Na^+ and Cu^+ ions, respectively. The Cu-O-Cu bond angle is 92.9° . This results in a small, ferromagnetic, nearest-neighbor (NN) exchange interaction. The antiferromagnetic next nearest-neighbor (NNN) interaction is the largest parameter in the spin Hamiltonian. An analysis of high-temperature susceptibility demonstrates the significance of interactions reaching up to fourth-nearest neighbors of a Cu^{2+} ion.⁹ The static susceptibility displays a broad maximum around 52 K, associated with the evolution of short-range antiferromagnetic correlations.⁹ Upon cooling, susceptibility and specific heat measurements show two magnetic phase transitions at 12 and 8 K. Neutron diffraction results⁹ demonstrate that the former transition is due to a noncollinear magnetic ordering with the propagation vector $(0.5, \zeta, 0)$ with $\zeta = 0.227$, similar to that of LiCu_2O_2 where $\zeta = 0.174$.³ This underscores the conclusion that lattice disorder (which is negligible in NaCu_2O_2) is not responsible for the helimagnetism in this class of compounds. The ordered moment of $0.56 \mu_B$ is reduced with respect to the full spin-1/2 moment due to quantum fluctuations. The latter transition might be related to spin canting.

While both Raman scattering⁷ and inelastic neutron scattering⁵ work on magnetic excitations in LiCu_2O_2 has

been reported, the magnetic dynamics of NaCu_2O_2 has thus far not been investigated. In this article, we report an investigation of magnetic excitations in NaCu_2O_2 by polarized Raman scattering. In the magnetically long-range ordered state, three distinct features attributable to magnetic excitations are observed. Two modes around 18 and 58 cm^{-1} are observed both with parallel in-chain and crossed polarizations. This points to significant interchain interactions. In addition, a broad maximum around 390 cm^{-1} is present in in-chain polarization only. The temperature dependences of the low-energy and the two high-energy modes are characteristic of one- and two-magnon excitations, respectively. Upon heating, the three magnetic modes disappear, and we observe a pronounced quasielastic response predominantly in the in-chain polarization channel. These results are discussed in the light of previous work on CuO_2 spin chain materials, especially recent neutron scattering data and model calculations on LiCu_2O_2 .⁵

The phonon spectrum of NaCu_2O_2 was also investigated as a function of temperature and light polarization. The observed modes agree well with those predicted by *ab-initio* lattice dynamical calculations, which allows us to identify the phonon eigenvectors at the zone center. Unusually strong two-phonon modes with an unconventional temperature dependence are also observed. These features may be related to a broad electronic mode around 500 cm^{-1} , which possibly arises from electronically active defects.

This article is organized as follows. In Section II, we describe technical details pertaining to the Raman experiments and the lattice dynamical calculations. Sections III.A and III.B contain Raman data on phonon and magnetic excitations, respectively, along with a discussion of possible mode assignments. Section IV provides a summary of our findings.

II. EXPERIMENTAL DETAILS AND LATTICE DYNAMICAL CALCULATIONS

The single crystals were grown using a self-flux method as described elsewhere.⁸ The chemical composition of the studied sample is close to the ideal stoichiometry, as discussed previously.⁹ Raman scattering measurements were performed in quasi-backscattering geometry with the excitation line $\lambda = 514.5$ nm of an Ar^+ laser. The laser power of 7 mW was focused to a 0.1 mm diameter spot on the sample surface. Stokes and anti-Stokes measurements confirmed that the incident radiation did not increase the temperature of the samples by more than a few K. Spectra of the scattered radiation were collected by a DILOR-XY triple spectrometer and recorded by a nitrogen cooled charge-coupled device detector with a spectral resolution less than ~ 1 cm^{-1} .

The optical phonon frequencies were calculated within the density functional theory using the VASP software package.¹¹ Projector augmented wave (PAW) potentials

with an energy cutoff of 283, 259, and 273 eV were used for O, Na, and Cu, respectively. The atomic coordinates were first optimized in the single unit cell. Then a (2,4,1) supercell, which is 2, 4, and 1 times larger in the respective a, b and c directions, was constructed and the coordinates of the 160 atoms were optimized again. For the dispersion relation calculations, two k-points in the a and b directions and one in the c direction were retained, while for the (2,4,1) supercell a single k-point was used. Supercell calculations are required in order for the magnitude of the force constants to become negligible (which happens beyond 10 Angstroms) as well as to calculate the phonon dispersions exactly instead of using an interpolation. A series of single point energy calculations, which give the Hellmann-Feynmann forces acting on all atoms in the supercell, were then performed on the structure obtained by displacing, one at a time, each of the 20 inequivalent atoms in positive and negative directions along the Cartesian axes. Finally, the dynamical matrix for any point in reciprocal space was generated and diagonalised.

III. RESULTS AND DISCUSSION

A. Phonons

Figure 1 displays Raman spectra in *bb*-, *ba*-, and *aa*-polarizations at 5 and 295 K. Most of the modes shown are of lattice vibrational origin. In order to assign these modes, we performed a group theoretical analysis as well as *ab-initio* lattice dynamical calculations following the description in Section II. NaCu_2O_2 has the space group Pnma, where all atoms have a 4c site symmetry. Apart from the acoustic ($B_{1u} + B_{2u} + B_{3u}$) modes, the factor group analysis yields the following Raman- and infrared-active modes: $10 A_g(\text{aa,bb,cc}) + 5 B_{1g}(\text{ab}) + 10 B_{2g}(\text{ac}) + 5 B_{3g}(\text{bc}) + 5 A_u + 9 B_{1u} + 4 B_{2u} + 9 B_{3u}$. Thus, in *bb*- and *aa*-geometries we expect 10 A_g modes, and in the *ba*-configuration 5 B_{1g} modes.

The observed peak frequencies are listed in Table I together with the calculated ones. Given that the calculation was performed without adjustable parameters, the agreement of observed and calculated frequencies is quite satisfactory. We can thus tentatively assign the observed modes to specific vibration patterns. Figures 2 and 3 provide a synopsis of the eigenvectors of the Raman-active modes resulting from the calculation. It can be seen that the highest-energy modes around 500 cm^{-1} are predominantly oxygen vibrations, as expected based on the small mass of the oxygen ion.

In both *aa*- and *bb*-polarizations we observe a total of 13 A_g modes. This number is larger than the expected 10 modes. Specifically, the highest-energy oxygen vibration around 560 cm^{-1} seems to be split into three modes, indicating different environments of oxygen ions in the crystal structure (see Fig. 7). This is either due to coherent deviations from the reported Pnma lattice

TABLE I: Comparison between experimental and calculated phonon frequencies of the Raman-active modes in a unit of cm^{-1} .

observed frequencies		calculated frequencies			
(aa),(bb)	(ab)	$10A_g$	$5B_{1g}$	$10B_{2g}$	$5B_{3g}$
55.7	55.7	42.2	41.4	47.2	
				80.6	79
114.6	114.6	93.5		91.8	109
142.5	142.5	131.7			
146.2	146.2	149.6	147.23	161.5	
164.6	164.6	181.1	169.3	197.3	167.9
217.5		254.5	253.1	253.4	289
317.4	317.4	405.8		393	
432.9		439.7	425.7	433.5	413
467.3	451.7			473	
501.9	501.9	510.2			
556.8	556.8	551.9			
566.6	566.6				
571.6	571.6			585.9	

symmetry too subtle to be discernible in the reported x-ray and neutron⁹ powder diffraction data, or to lattice defects. In *ab*-polarization 11 modes are observed, a number that is also larger than the symmetry-allowed 5 B_{1g} modes. Our calculations show that the estimated frequency separation between the A_g and B_{1g} modes is only $1 - 2 \text{ cm}^{-1}$. This lies within our spectral resolution of $\sim 1 \text{ cm}^{-1}$. It is therefore difficult to assess whether the modes observed in *ab*-polarization are pure B_{1g} modes, or whether they are due to an admixture of A_g modes due to polarization leakage caused by lattice defects and/or other mechanism.

The temperature dependence of the peak frequencies and linewidths of representative phonons, extracted by fitting the corresponding spectra to Lorentzian profiles, is shown in Fig. 4. Nearly all phonon modes exhibit a similar behavior. With decreasing temperature the peak frequencies harden and the linewidths narrow gradually, before saturating at about 70 K. This behavior is commonly observed as a consequence of lattice anharmonicity. However, two phonons exhibit phenomena not attributable to anharmonic effects alone. First, the linewidth of the 146 cm^{-1} mode, which according to the calculation mostly involves a *b*-axis vibration of the Cu^{1+} ions against the rest of the lattice (Fig. 3), exhibits a subtle but distinct drop upon cooling from 50 K to the lowest temperatures (see the arrow in Fig. 4). As the CuO_2 chains vibrate in unison, a strong spin-phonon coupling is not expected, and the relationship of this subtle anomaly to the development of magnetic correlations is not obvious. Second, the 502 cm^{-1} oxygen vibration shows an asymmetric lineshape, which appears to be due to an anti-resonance with a broad electronic mode centered around 500 cm^{-1} . The origin of the electronic mode will be addressed in Section III.B below.

Here we draw attention to the unusual behavior of the two-phonon peak around 1000 cm^{-1} , which is probably an overtone of the 502 cm^{-1} mode (Fig. 1). In *bb*-polarization and at 5 K, the integrated intensity of the two-phonon peak is nearly an order of magnitude higher than that of the one-phonon peak. At room temperature, the two-phonon peak *decreases* strongly in intensity. In contrast, the ratio of the integrated intensities of one- and two-phonon modes for the *aa*-configuration is only ~ 0.3 in the temperature regime investigated. Since two-phonon excitations are usually weak and hardly change with increasing temperature, the behavior of this mode is quite surprising. Qualitatively similar (albeit less pronounced) effects were observed in corner-sharing copper oxide chain systems, and interpreted in terms of a Fröhlich interaction mechanism.^{12,13} This mechanism can also lift the selection rules such that infrared-active modes may become observable by Raman spectroscopy. This might explain the observed extra phonon modes. A quantitative understanding of the two-phonon modes of NaCu_2O_2 remains a subject of future work.

B. Magnetic excitations

Magnetic excitations in the Raman spectra can be identified by virtue of their temperature and polarization dependences. The upper panel of Fig. 1 shows a substantial temperature-induced rearrangement of spectral weight in in-chain *bb*-polarization. The low-energy part of the spectrum that is affected by this redistribution is highlighted in Fig. 5. Upon cooling, a broad quasielastic background is progressively replaced by a more structured spectrum. At 5 K, three features attributable to magnetic excitations emerge: (i) an $\sim 50 \text{ cm}^{-1}$ wide peak centered at 390 cm^{-1} ; (ii) a weaker peak with an asymmetric lineshape extending from about 50 to 170 cm^{-1} ; (iii) and a sharp peak around 17 cm^{-1} . The latter two features are also present in *ab*-polarization (see the middle panel of Fig. 1). Their temperature dependence is highlighted in Figs. 6 and 7, respectively. The magnetic Raman operator is given by $\mathcal{R} \propto S_i \cdot S_j$,¹ so that magnetic Raman scattering is dominant in the polarization where there are substantial exchange paths. The observation of features (ii) and (iii) in both *bb*- and *ba*-polarizations thus indicates that they are appreciably affected by interchain coupling.

Before discussing these features in detail, we recall the salient properties of the spin Hamiltonian of NaCu_2O_2 .⁹ The largest exchange coupling parameter is the antiferromagnetic NNN coupling along the spin chains ($J_2 = 62.6 \text{ cm}^{-1}$). The helix structure is induced by a frustrating ferromagnetic NN interaction $J_1 = 11.4 \text{ cm}^{-1}$. Longer-range exchange interactions along the chains and/or interactions between spins within a closely spaced pair of spin chains are also required to obtain a good fit to the magnetic susceptibility and the propagation vector of the helix structure.

The magnetic excitations of NaCu_2O_2 have thus far not been studied, but an inelastic neutron scattering study has recently addressed the low-energy spin excitations in LiCu_2O_2 .⁵ Based on model calculations,¹⁴ the largest parameter in the spin Hamiltonian, J_2 , is expected to be very similar in the two systems. From the $\sim 30\%$ smaller pitch angle of the magnetic helix in NaCu_2O_2 one can infer a correspondingly smaller NN coupling J_1 . This is expected, because the Cu-O-Cu bond angle of NaCu_2O_2 is closer to 90° , and it is consistent with the data currently available on this compound. Although there may be further subtle differences between the spin Hamiltonians of both compounds, the neutron scattering data and model calculations reported for LiCu_2O_2 can thus serve as a useful guideline for the interpretation of our data.⁵ Note that the Raman data presented here cover the high-energy and low-energy segments of the spin wave spectrum not probed by the neutron experiments on LiCu_2O_2 . Both data sets can thus be regarded as complementary in this respect as well.

We first discuss the two broad modes centered at 70 and 390 cm^{-1} . The temperature dependence of the former feature is shown in more detail in Fig. 5. It persists well into the paramagnetic state and merges into the background at temperatures exceeding about 80 K. The 390 cm^{-1} feature persists to even higher temperatures in excess of 150 K, without a strong renormalization of its lineshape (Fig. 7). This is the temperature dependence expected for two-magnon Raman scattering in low-dimensional magnets, where short-range spin correlations persist well into the paramagnetic state. The presence of the higher-energy two-magnon peak in *bb*-polarization, and its absence in *ab*-polarization, confirm that the magnetic zone-boundary energy is determined predominantly by exchange interactions within a single spin chain, as expected based on the discussion above. Its energy is expected to be slightly below twice the magnetic zone-boundary energy, due to magnon-magnon interactions. This is indeed the case, as the zone-boundary energy computed in Ref. 5 is 26 meV ($= 210\text{ cm}^{-1}$).

The presence of a second two-magnon feature is more unusual, but it can be understood as a consequence of the helical spin correlations present in NaCu_2O_2 and LiCu_2O_2 . The helical spin structure and the four-atom basis in the magnetic unit cell give rise to a complex spin wave spectrum (Fig. 6a of Ref. 5), with several magnon branches exhibiting either maxima or minima in the energy range $8\text{--}12\text{ meV}$ ($65\text{--}97\text{ cm}^{-1}$) for LiCu_2O_2 . Because of the lower value of J_1 (see discussion above), this energy scale is expected to be reduced in NaCu_2O_2 . The high two-magnon density of states due to the vanishing spin-wave velocity at these extrema of the dispersion relation naturally explains the second two-magnon Raman peak. The observation of this peak in both *bb*- and *ab*-polarization indicates that magnons in the energy range around 10 meV are significantly influenced by interchain exchange interactions within a pair of closely spaced chains. This agrees with the findings of Ref.

5, but seems incompatible with the prediction of negligible interchain exchange interactions based on LDA calculations.⁴

We will now address the origin of the peak at 18 cm^{-1} . As shown in detail in Fig. 6, the peak broadens and shifts to lower frequency upon heating, and it vanishes above the magnetic transition temperature. This behavior is characteristic of one-magnon excitations. A one-magnon excitation with almost identical energy has been observed in CuGeO_3 , a spin-Peierls compound also based on edge-sharing copper oxide chains, in magnetic fields high enough to stabilize a phase with an incommensurate modulation of both the spin density and the crystal lattice.¹⁵ However, the presence of both spin and lattice modulations has made it difficult to arrive at a conclusive interpretation of the nature of this mode and the origin of its Raman-activity.^{15,16,17} One-magnon modes of comparable energies have also been observed in Raman scattering experiments on the two-dimensional antiferromagnet La_2CuO_4 .¹⁸ These zone-center transverse magnon modes are Raman active by virtue of spin-orbit coupling, which manifests itself in an exchange anisotropy two orders of magnitude smaller than the isotropic Cu-O-Cu superexchange interaction.

The most straightforward interpretation of the 18 cm^{-1} peak is based on a transverse magnon at $q = 0$. This is consistent with neutron scattering measurements on LiCu_2O_2 , which tentatively indicate a magnon gap of comparable magnitude.⁵ If this scenario is valid, the size of this gap constitutes a large fraction of the isotropic superexchange interaction. This may at first seem surprising in view of the nearly quenched orbital moment of the Cu^{2+} ion. However, prior work on edge-sharing copper oxide chain systems has experimentally demonstrated substantial superexchange anisotropies.¹⁹ The surprisingly large relative magnitude of the non-isotropic part of the exchange interaction can be understood based on electronic structure calculations for the 90° Cu-O-Cu bond geometry.¹⁹ A zone-center transverse magnon is therefore a plausible origin of the 18 cm^{-1} peak.

An alternative interpretation of this peak is in terms of a longitudinal magnon. Such excitations are usually heavily damped, but can live long enough to be probed near quantum critical points. Indeed, longitudinal magnons have recently been observed in Raman scattering experiments²⁰ on the coupled spin-tetrahedra system $\text{Cu}_2\text{Te}_2\text{O}_5\text{Br}_2$, which exhibits incommensurate helical order and a spin excitation spectrum not unlike those of NaCu_2O_2 .^{21,22} Because of the sizable ordered moment of NaCu_2O_2 ,⁹ this scenario is less plausible. However, a conclusive assignment of the 18 cm^{-1} peak will have to await neutron spectroscopy experiments on NaCu_2O_2 akin to those that have led to the identification of longitudinal magnons in other systems.^{23,24,25} Another open question concerns the temperature dependence of the frequency and intensity of the 18 cm^{-1} mode. In contrast to one-magnon excitations in most collinear magnets, whose frequency and intensity roughly scale with the or-

der parameter, we observe a temperature-linear behavior of these quantities (Fig. 6). Detailed model calculations for the observed helical magnetic structure are required to address the origin of this behavior.

At high temperatures, the one- and two-magnon peaks are replaced by an intense quasielastic peak due to overdamped spin excitations. Similar phenomena have been studied in other quasi-one-dimensional magnets such as CuGeO_3 .^{26,27} Using a hydrodynamic description of the correlation function,¹ the quasielastic Raman peak is well described by a Lorentzian profile $I(\omega) \propto C_m T^2 D_T k^2 / [\omega^2 + (D_T k^2)^2]$, where k is the scattering wave vector, D_T the thermal diffusion constant, and C_m the magnetic specific heat. Figure 8 displays a representative fit of the quasielastic response to a Lorentzian profile at 295 K. The inset of Fig. 8 shows the temperature dependence of the scattering amplitude, which increases rapidly with increasing temperature and then saturates around 200 K. This is the same temperature at which the higher-energy two-magnon peak vanishes, heralding the disappearance of short-range spin-spin correlations. Here we note that deviations from the Lorentzian profile are discernible above 100 cm^{-1} (not shown here). While this is partly due to an ambiguity in determining the scattering background, it may also reflect interference from an additional scattering channel at higher energies, which we will now discuss.

Figure 7 indeed shows a broad, weakly temperature independent peak centered around 500 cm^{-1} , the tail of which may well extend down to about 100 cm^{-1} . The peak is observed almost exclusively in the bb -polarization channel, although some traces may also be present in the other polarizations. As already mentioned in Section III.A, the oxygen vibration at 502 cm^{-1} exhibits a pronounced anti-resonance behavior with this mode. The peak does not shift as the laser frequency is varied, so that luminescence can be ruled out. Since the strong anisotropy, the nearly temperature dependent spectral weight, and the featureless shape of the peak are inconsistent with multiphonon scattering, it is probably of electronic origin.

An unambiguous assignment of this peak is not possible based on the data at hand. A priori, one has to consider orbital, charge, and magnetic excitations of the electrons. Raman scattering experiments have recently uncovered evidence of orbital excitations in transition metal oxides with t_{2g} valence electrons at energies ranging from ~ 500 to $\sim 2000 \text{ cm}^{-1}$,^{28,29} but orbital excitations for the e_g electron of a Cu^{2+} ion are expected to occur at much higher energies. Because of the presence of both Cu^{1+} and Cu^{2+} ions in NaCu_2O_2 , one might also consider low-energy charge excitations as the origin of the peak. The eigenvectors of both of the phonons exhibit-

ing anomalous behavior suggest that the corresponding vibrations modulate Cu^{1+} - Cu^{2+} charge-transfer excitations. However, band structure calculations and photoemission data for LiCu_2O_2 indicate considerably larger energies for such excitations.³⁰ Finally, a spinon continuum extending beyond the magnon bandwidth is expected on general grounds in one-dimensional magnets. Indeed, Raman scattering from such continuum excitations has been reported for edge-sharing copper oxide chains.¹² In this scenario, the phonon anomalies discussed in Section III.A may be consequences of a spin-phonon interaction, also invoked to explain phonon anomalies in CuGeO_3 .³¹ While we consider this as the most likely interpretation of the 500 cm^{-1} peak, we cannot rule out entirely that it is a consequence of defects in the NaCu_2O_2 crystal structure. As the Na/Cu ratio determined in prior work on NaCu_2O_2 was stoichiometric within an error margin of about 2%,⁹ defects on these atomic sites can be present only in very small concentrations. Oxygen defects can, however, not be ruled out. Whatever their origin, it is conceivable that electronically active lattice defects could give rise to charge carriers in shallow traps, which shake off spin excitations propagating along the b -direction when excited into the conduction band, giving rise to a broad Raman peak. Further work with other probes is required to conclusively establish the origin of the 500 cm^{-1} peak.

IV. CONCLUSIONS

To conclude, we have presented a detailed study of the phonon spectrum and the magnetic response of the helically ordered spin-chain system NaCu_2O_2 using Raman spectroscopy. Based on lattice dynamical calculations, most of the phonon modes could be assigned. Several spectral features originating from magnetic excitations were observed as well. The rich magnetic Raman spectrum of NaCu_2O_2 is unusual for a quasi-one-dimensional magnet. However, a comparison to model calculations and neutron scattering data on the isostructural compound LiCu_2O_2 and prior Raman scattering work on other copper oxide chain systems yields plausible interpretations of all of the observed modes.

Acknowledgments

We thank Manuel Cardona, Peter Horsch, and Karin Schmalzl for useful discussions, and D. Richard and A. Filhol for technical assistance.

¹ P. Lemmens, G. Güntherodt, and C. Gros, Phys. Rep. **375**, 1 (2003) and references therein.

² S. A. Zvyagin, G. Cao, Y. Xin, S. McCall, T. Caldwell, W.

- Moulton, L.-C. Brunel, A. Angerhofer, and J. E. Crow, *Phys. Rev. B* **66**, 064424 (2002).
- ³ T. Masuda, A. Zheludev, A. Bush, M. Markina, and A. Vasiliev, *Phys. Rev. Lett.* **92**, 177201 (2004).
- ⁴ A. A. Gippius, E. N. Morozova, A. S. Moskvina, A. V. Zalessky, A. A. Bush, M. Baenitz, H. Rosner, and S.-L. Drechsler, *Phys. Rev. B* **70**, 020406 (2004).
- ⁵ T. Masuda, A. Zheludev, B. Roessli, A. Bush, M. Markina, and A. Vasiliev, *Phys. Rev. B* **72**, 014405 (2005).
- ⁶ T. Masuda, A. Zheludev, A. Bush, M. Markina, and A. Vasiliev, *Phys. Rev. Lett.* **94**, 039706 (2005); S.-L. Drechsler, J. Malek, J. Richter, A. S. Moskvina, A. A. Gippius, and H. Rosner, *Phys. Rev. Lett.* **94**, 039705 (2005).
- ⁷ K.-Y. Choi, S. A. Zvyagin, G. Cao, and P. Lemmens, *Phys. Rev. B* **69**, 104421 (2004).
- ⁸ A. Maljuk, A. B. Kulakov, M. Sofin, L. Capogna, J. Strempfer, C. T. Lin, M. Jansen, and B. Keimer, *J. Cryst. Growth* **263**, 338 (2004).
- ⁹ L. Capogna, M. Mayr, P. Horsch, M. Raichle, R. K. Kremer, M. Sofin, A. Maljuk, M. Jansen, and B. Keimer, *Phys. Rev. B* **71**, 140402(R) (2005).
- ¹⁰ P. Horsch, M. Sofin, M. Mayr, and M. Jansen, *Phys. Rev. Lett.* **94**, 076403 (2005).
- ¹¹ G. Kresse and J. Furthmüller, *Phys. Rev. B* **54**, 11169 (1996).
- ¹² O. V. Misochko, S. Tajima, C. Urano, H. Eisaki, and S. Uchida, *Phys. Rev. B* **53**, R14733 (1996).
- ¹³ M. V. Abrashev, A. P. Litvinchuk, C. Thomsen, and V. N. Popov, *Phys. Rev. B* **55**, R8638 (1997).
- ¹⁴ Y. Mizuno, T. Tohyama, S. Maekawa, T. Osafune, N. Motoyama, H. Eisaki, and S. Uchida, *Phys. Rev. B* **57**, 5326 (1998).
- ¹⁵ I. Loa, S. Gronemeyer, C. Thomsen, and R. K. Kremer, *Solid State Commun.* **111**, 181 (1999).
- ¹⁶ M. Enderle, H. M. Rønnow, D. F. McMorrow, L.-P. Regnault, G. Dhalle, A. Revcholevski, P. Vorderwisch, H. Schneider, P. Smeibidl, and M. Meißner, *Phys. Rev. Lett.* **87**, 177203 (2001).
- ¹⁷ G. S. Uhrig, F. Schönfeld, and J. P. Boucher, *Europhys. Lett.* **41**, 431 (1998).
- ¹⁸ A. Gozar, B. S. Dennis, G. Blumberg, S. Komiya, and Y. Ando, *Phys. Rev. Lett.* **93**, 027001 (2004).
- ¹⁹ V. Kataev, K.-Y. Choi, M. Grüninger, U. Ammerahl, B. Büchner, A. Freimuth, and A. Revcholevski, *Phys. Rev. Lett.* **86**, 2882 (2001).
- ²⁰ C. Gros, P. Lemmens, M. Vojta, R. Valent, K.-Y. Choi, H. Kageyama, Z. Hiroi, N. V. Mushnikov, T. Goto, M. Johnsson, and P. Millet, *Phys. Rev. B* **67**, 174405 (2003).
- ²¹ P. Lemmens, K.-Y. Choi, E. E. Kaul, C. Geibel, K. Becker, W. Brenig, R. Valenti, C. Gros, M. Johnsson, P. Millet, and F. Mila, *Phys. Rev. Lett.* **87**, 227201 (2001).
- ²² O. Zaharko, A. Daoud-Aladine, S. Streule, J. Mesot, P.-J. Brown, and H. Berger, *Phys. Rev. Lett.* **93**, 217206 (2004); J.S. Crowe, S. Majumdar, M. R. Lees, D. McK. Paul, R. I. Bewley, S. J. Levett, and C. Ritter, *Phys. Rev. B* **71**, 224430 (2005).
- ²³ Z. Tun, W. J. L. Buyers, R. B. Armstrong, K. Hirakawa, and B. Briat, *Phys. Rev. B* **42**, 4677 (1990).
- ²⁴ A. Zheludev, M. Kenzelmann, S. Raymond, T. Masuda, K. Uchinokura, and S.-H. Lee, *Phys. Rev. B* **65**, 014402 (2002).
- ²⁵ B. Lake, D. A. Tennant, and S. E. Nagler, *Phys. Rev. B* **71**, 134412 (2005).
- ²⁶ H. Kuroe, J. Sasaki, T. Sekine, N. Koide, Y. Sasago, K. Uchinokura, and M. Hase, *Phys. Rev. B* **55**, 409 (1997).
- ²⁷ W. Brenig, *Phys. Rev. B* **56**, 2551 (1997).
- ²⁸ S. Miyasaka, S. Onoda, Y. Okimoto, J. Fujioka, M. Iwama, N. Nagoaso, and Y. Tokura, *Phys. Rev. Lett.* **94**, 076405 (2005).
- ²⁹ C. Ulrich, A. Gössling, M. Grüninger, M. Guennou, H. Roth, M. Cwik, T. Lorenz, G. Khaliullin, and B. Keimer, *cond-mat/0503106* (unpublished).
- ³⁰ D. A. Zatsépin, V. R. Galapov, M. A. Korotin, V. V. Fedorenko, E. Z. Kurmaev, S. Bartkowski, M. Neumann, and R. Berger, *Phys. Rev. B* **57**, 4377 (1998).
- ³¹ I. Loa, S. Gronemeyer, C. Thomsen, and R. K. Kremer, *Solid State Commun.* **99**, 231 (1996).

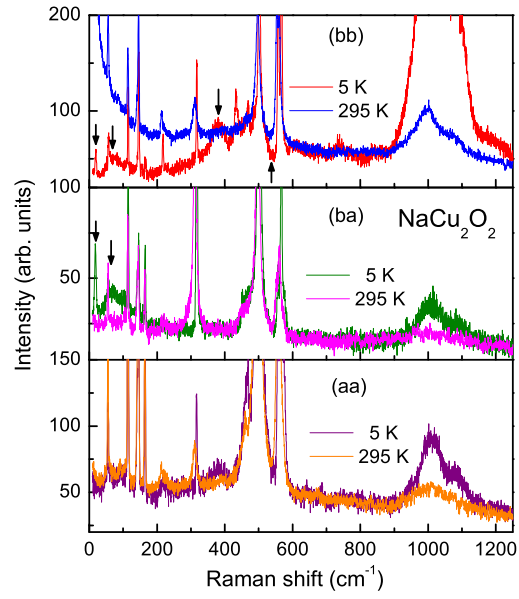


FIG. 1: (Color online) Polarization dependence of Raman spectra at 5 and 295 K in bb -, ba -, and aa - polarizations, respectively. The downward vertical arrows indicate magnetic excitations while the upward one denotes a Fano-shaped dip corresponding to the phonon at 502 cm^{-1} .

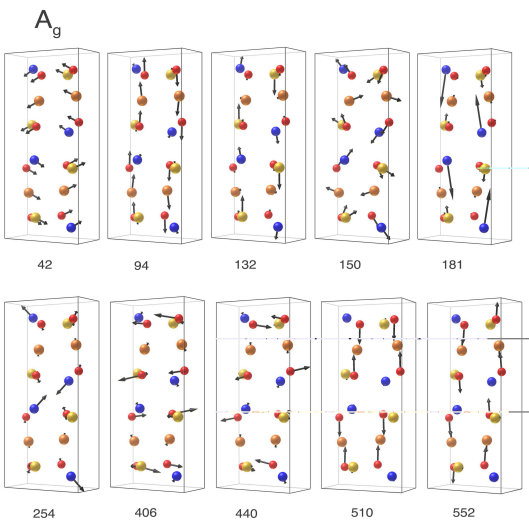


FIG. 2: (Color online) Calculated normal frequencies and eigenvectors of the A_g -symmetry modes. The relative amplitude of the vibrations (arrow length) is correct within each mode. For the sake of clarity a multiplication factor has been applied to some modes. The red balls stand for the oxygen ions, the blue ones for sodium, the yellow ones for the Cu^{+2} , and the orange ones for the Cu^{+1} .

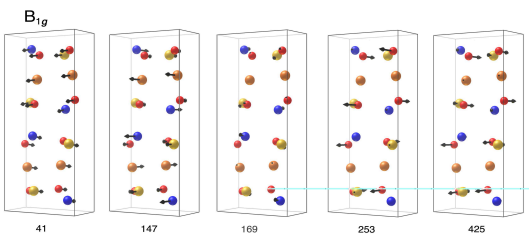


FIG. 3: (Color online) Calculated normal frequencies and eigenvectors of the B_{1g} -symmetry modes. The relative amplitude of the vibrations (arrow length) is correct within each mode. For the sake of clarity a multiplication factor has been applied to some modes.

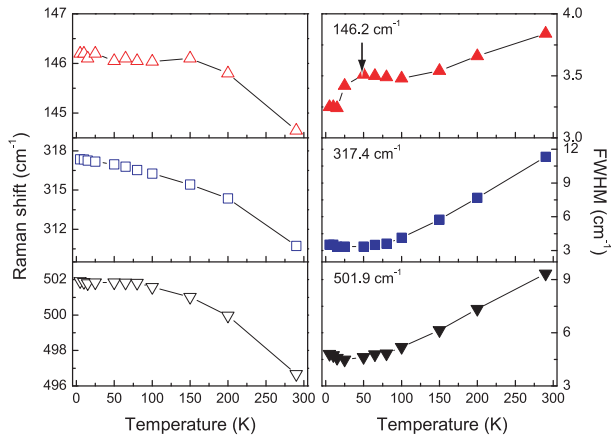


FIG. 4: (Color online) (Left panel) Temperature dependence of the peak frequencies of selected phonons. (Right panel) Phonon linewidths as a function of temperature.

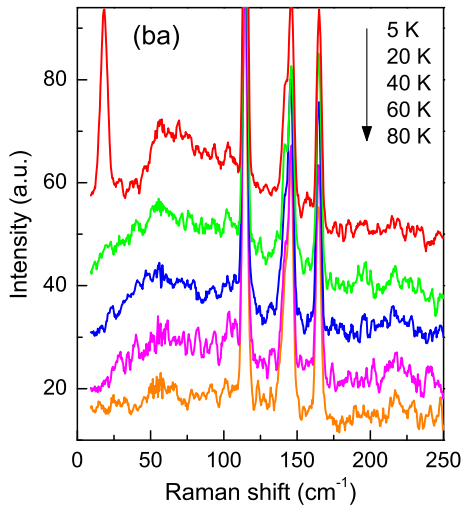


FIG. 5: (Color online) Temperature dependence of magnetic Raman spectra in ba -polarization at 5, 20, 40, 60, and 80 K (from upper to lower curve).

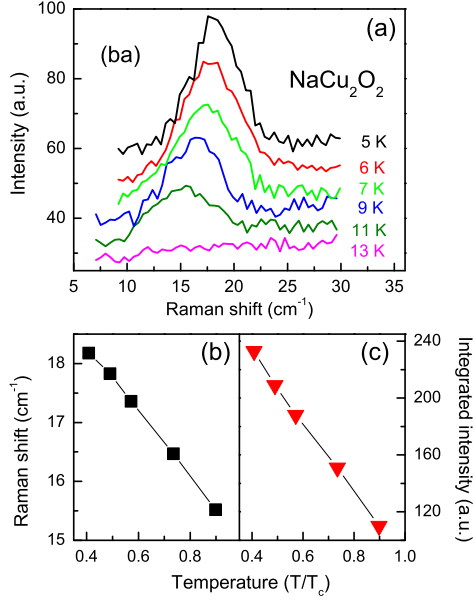


FIG. 6: (Color online) (a) Low-frequency magnetic Raman spectra in ba -polarization as a function of temperature. (b,c) Temperature dependence of the peak position and integrated intensity on a reduced temperature scale, respectively.

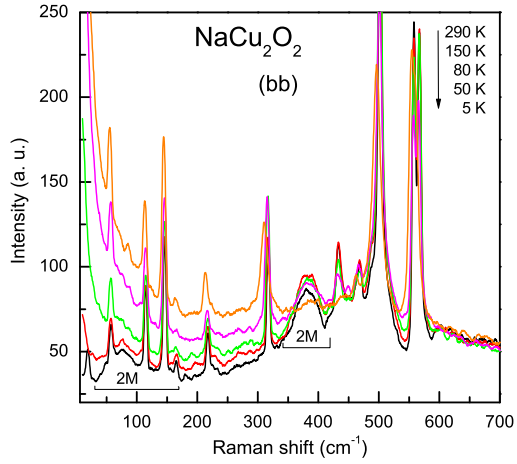


FIG. 7: (Color online) Raman spectra in bb -polarization as a function of temperature; 290, 150, 80, 50, and 5 K from upper to lower curve.

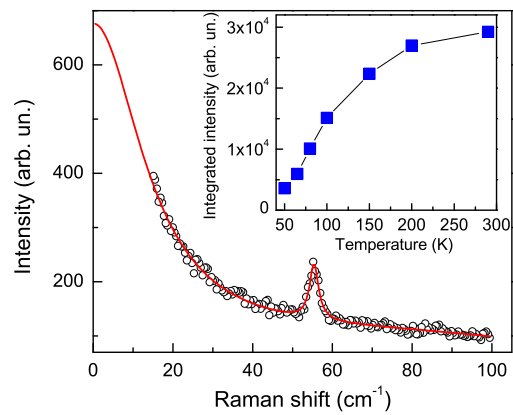


FIG. 8: (Color online) Result of a fit of the quasielastic response to a Lorentzian profile at 295 K. Inset: Temperature dependence of the integrated scattering intensity of this profile.